Finite Elements in Analysis and Design 135 (2017) 11–21

Contents lists available at ScienceDirect

Finite Elements in Analysis and Design

journal homepage: www.elsevier.com/locate/finel

Sensitivity analysis for radiofrequency induced thermal therapies using the complex finite element method

Juan F. Monsalvo[a], Manuel J. García[a,b,*], Harry Millwater[b], Yusheng Feng[b]

[a] Applied Mechanics Research Group, Universidad EAFIT, Medellín, Colombia
[b] Mechanical Engineering Department, University of Texas at San Antonio, TX, USA

ARTICLE INFO

Keywords:
Sensitivity analysis
Complex Taylor series expansion
Bioheat transfer equation
Radio frequency ablation
Liver cancer treatment

ABSTRACT

In radiofrequency induced thermal procedures for cancer treatment, the temperature of the cancerous tissue is raised over therapeutic values while maintaining the temperature of the surrounding tissue at normal levels. In order to control these temperature levels during a thermal therapy, it is important to predict the temperature distribution over the region of interest and analyze how the variations of the different parameters can affect the temperature in the healthy and damaged tissue. This paper proposes a sensitivity analysis of the radiofrequency induced thermal procedures using the complex Taylor series expansion (CTSE) finite element method (ZFEM), which is more accurate and robust compared to the finite difference method. The radiofrequency induced thermal procedure is modeled by the bioheat and the Joule heating equations. Both equations are coupled and solved using complex-variable finite element analysis. As a result, the temperature sensitivity with respect to any material property or boundary condition involved in the process can be calculated using CTSE.

Two thermal therapeutical examples, hyperthermia and ablation induced by radio frequency, are presented to illustrate the capabilities and accuracy of the method. Relative sensitivities of the temperature were computed for a broad range of parameters involved in the radiofrequency induced thermal process using ZFEM. The major feature of the method is that it enables a comprehensive evaluation of the problem sensitivities, including both model parameters and boundary conditions. The accuracy and efficiency of the method was shown to be superior to the finite difference method. The computing time of a complex finite element analysis is about 1.6 times the computing time of real finite element analysis; significantly lower than the 2 times of forward/backward finite differencing or 3 times of central differencing. It was found that the radiofrequency hyperthermia procedure is very sensitive to the electric field and temperature boundary conditions. In the case of the radiofrequency ablation procedure, the cooling temperature of the electrodes has the highest liver/tumor temperature sensitivity. Also, thermal and electrical conductivities of the healthy tissue were the properties with the highest temperature sensitivities. The result of the sensitive analysis can be used to design very robust and safe medical procedures as well as to plan specific patient procedures.

1. Introduction

A radiofrequency induced thermal procedure is a minimally invasive clinical method for the treatment of hepatocellular carcinoma that consists of the heating of biological tissues through the emission of an external electric field. The radiofrequency induced thermal procedure is used when the tumor or other dysfunctional tissues are not surgically resectable due to the location or the potential of significant collateral damage in the surgical process. Radio frequency ablation can be used to treat tumors in the liver as well as those in other organ sites such as lung, kidney, pancreas and bone.

The goal of a radiofrequency induced thermal treatment is to raise the temperature of the tumor to a value in the range from (42 – 46)°C for hyperthermia therapy, or to a value in the range from (50 – 100)°C for radiofrequency ablation therapy. The temperature field is applied for certain time so that the tumor tissues are destroyed while keeping the temperature in the healthy tissue region below critical temperature to avoid unwanted damage [1–3]. The success of either hyperthermia and ablation induced by radio frequency depend on: (i) how well the temperature field is controlled and optimized to ensure the temperature is high enough to destroy the cancer cells in the tumor region (ii) how to minimize the damage in the healthy tissues surrounding the

* Corresponding author at: Applied Mechanics Research Group, Universidad EAFIT, Medellín, Colombia.
E-mail addresses: jmonsa13@eafit.edu.co (J.F. Monsalvo), manuel.garciaruiz@utsa.edu (M.J. García), harry.millwater@utsa.edu (H. Millwater), yusheng.feng@utsa.edu (Y. Feng).

http://dx.doi.org/10.1016/j.finel.2017.07.001
Received 14 February 2017; Received in revised form 1 June 2017; Accepted 2 July 2017
Available online 13 July 2017
0168-874X/

tumor with reasonable margin prescribed by an oncologist or surgeon.

The thermal modeling of the radiofrequency induced thermal treatment has been studied by several researchers with Pennes [4] the first to introduce a mathematical equation explaining the heat transfer present in a biological tissue. This equation is known as the bioheat transfer equation. Tunç et al. [5] applied the bioheat transfer equation in the analysis of hyperthermia treatments. Chang and Nguyen developed a model to predict the size of the thermal lesions created by the radiofrequency induced thermal procedure using the Arrhenius equation which relates the temperature and the exposure time, using a first order kinetics relationship [6]. Fuentes et al. compared the thermal damage region, recreated in a computer simulation, with the radiofrequency induced thermal procedure in an *in vitro* perfused bovine liver model, finding a good correlation between the two damage regions [1]. In addition, the bioheat transfer in some organs may need a hyperbolic term to account for finite time dispersion of heat energy [7].

Despite significant research efforts, the prediction of the temperature distribution is still an important issue in the reliability and effectiveness of the treatment. Since the human body is a complex blend of tissue with heterogeneous electric and thermal characteristics, it is a difficult task to predict and control the temperature distribution and to determine the optimum heating configuration during therapy. Recent advances in this direction include the development of a patient-specific image-based 3D model for thermal ablation simulation to optimize treatment efficacy [8]. Also, Schumann et al. proposed an access path determination method, for radiofrequency ablation planning, based on image processing and numerical optimization [9]. Therefore, it is important to develop a tool capable of predicting the thermal results given the variation of the material properties and the radiofrequency induced thermal variables. Hence, a thorough sensitivity analysis of each variable involved in the process will allow one to identify those variables with the largest impact on the tumor temperature distribution. The Complex Taylor Series Expansion (CTSE) method was used here to perform this analysis. It was first proposed by [10] and [11]. [12] were the first to obtain a method to approximate derivatives of real functions using complex variables. The CTSE method calculates the first derivative with respect a parameter by perturbing the parameter along the imaginary axes. There is no difference operation involved, and therefore it avoids the cancellation error presented in the Finite Difference Method (FDM). This allows the method to be step size independent, easy to implement and highly accurate. The method has proven to be very attractive in applications where a sensitivity analysis is required, and it has been applied in several fields of engineering as: the computation of sensitivity derivatives of NavierStokes equations [13], shape sensitivity analysis [14], fatigue sensitivity analysis [15], fracture mechanics [16–19], nonlinear problems in plasticity [20] and creep [21], aerodynamics [22,23], structural dynamics [24,25], and nonlinear structural analysis [26], among others. However, the CTSE has not been exploited in bioengineering or medical research.

In this paper, a simplified 2D geometry of the radiofrequency induced thermal process was modelled using the bioheat transfer equation coupled with the Joule heating equation. The sensitivity was calculated using CTSE, and the results were compared with the sensitivity found using the finite difference method in order to demonstrate the superior step size independence of the CTSE method.

2. Radiofrequency induced thermal process

A simplified 2D model of the radiofrequency ablation, adopted and modified from [27], is shown in Fig. 1. The domain Ω is composed of two subdomains, the healthy tissue domain Ω_1, and the tumor domain Ω_2. A point $\boldsymbol{x} = (x, y) \in \Omega$, will have different properties depending on whether it is located in the tumor, $\boldsymbol{x} \in \Omega_2$, or in the healthy tissue, $\boldsymbol{x} \in \Omega_1$. The boundary of the domain $\partial\Omega$ is composed of four parts

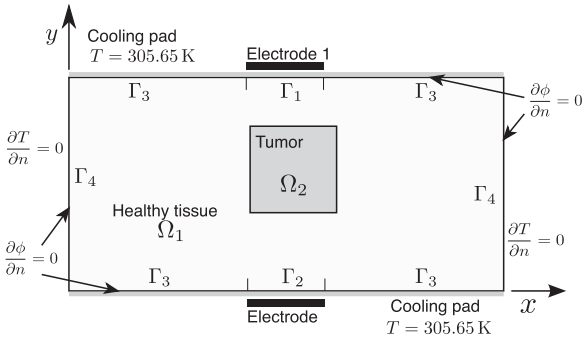

Fig. 1. A simplified 2D model of a radiofrequency induced thermal treatment (hyperthermia) with an embedded tumor.

$\partial\Omega = \Gamma_1 + \Gamma_2 + \Gamma_3 + \Gamma_4$. The electric field is generated from two electrodes located on the top Γ_1 and bottom Γ_2 of the healthy tissue, generating a voltage gradient. The top and bottom of the healthy tissue Γ_3 are covered with a cooling pad that preserves a constant temperature at the surface. The left and right side Γ_4 are assumed insulated surfaces. A detail description of the geometry is presented in Section 4.

The radiofrequency induced thermal treatment can be described as the coupling of two physical phenomena. The first is the heat induced by the electric field generated from the electrodes; the second is the heat transfer in the tissue and considers the metabolic heat, perfusion rate and the heat produced by the electric field. The combination of these two models allows one to predict the temperature field distribution on the domain (organ). A quasi-static electric field approximation was used due to the fact that the wave length of the radiofrequency is much greater compared to the depth of the computational domain, therefore, the free charge continuity equation takes the following form [28],

$$\nabla\cdot\boldsymbol{J}(\boldsymbol{x}) = 0, \tag{1}$$

where the electric current density $\boldsymbol{J} = \boldsymbol{J}(\boldsymbol{x})[\mathrm{A/m^2}]$ is related to the electric field through the Ohm's law

$$\nabla\cdot\sigma(\boldsymbol{x})\boldsymbol{E}(\boldsymbol{x}) = 0. \tag{2}$$

Here, $\sigma = \sigma(\boldsymbol{x})$ [s/m] is the tissue electrical conductivity and $\boldsymbol{E} = \boldsymbol{E}(\boldsymbol{x})$ [V/m] denotes the electric field. The electric field can be defined as the gradient of the electric potential $\phi(\boldsymbol{x})$ [V]

$$\boldsymbol{E}(\boldsymbol{x}) = \nabla\phi(\boldsymbol{x}). \tag{3}$$

Substituting Eq. (3) into Eq. (2) yields the governing electric potential equation,

$$\nabla\cdot\sigma(\boldsymbol{x})\nabla\phi(\boldsymbol{x}) = 0. \tag{4}$$

When the electric conductivity σ is constant over the domain, Eq. (4) is transformed into the Laplace equation $\sigma\nabla^2\phi = 0$. However, this is not the case in the present study as the healthy tissue and tumor tissue have different physical properties. The boundary conditions necessary to solve Eq. (4) are as follows: a Dirichlet boundary condition with the value of the electric potential relative to ground is specified on each electrode Γ_1, Γ_2. A Newman boundary condition equal to zero, $\frac{\partial\phi}{\partial n} = 0$ representing an ideal electrical isolation, is specified on the remaining external boundaries Γ_3, Γ_4, see Fig. 1. The differential in electric potential produces an electric current through the tissue and releases heat. This process is called Joule heating and is also referred to as Ohmic or resistive heating. The amount of heat released is proportional to the square of the current, or in terms of the electric field

$$\begin{aligned} Q_J(\boldsymbol{x}) &= \sigma(\boldsymbol{x})\boldsymbol{E}(\boldsymbol{x})\cdot\boldsymbol{E}(\boldsymbol{x}) \quad \text{or} \\ Q_J(\boldsymbol{x}) &= \sigma(\boldsymbol{x})\|\nabla\phi(\boldsymbol{x})\|^2. \end{aligned} \tag{5}$$

On the other hand, the temperature distribution inside the healthy and the tumor tissue is described by the bioheat transfer equation also known as the Pennes equation [4]. This equation has an added source

term $Q_J(\boldsymbol{x})$ [W/m] which is a product of the Joule heating. The steady state version of the bioheat transfer equation is

$$\lambda\nabla^2 T(\boldsymbol{x}) + \rho_b C_b G_b[T_b - T(\boldsymbol{x})] + Q_m(\boldsymbol{x}) + Q_J(\boldsymbol{x}) = 0, \tag{6}$$

in which T [K] denotes the temperature, $\lambda(\boldsymbol{x})$ [W/mK] is the thermal conductivity, ρ_b [kg/m^3] denotes the blood density, C_b [J/kg K] is the specific heat capacity of the blood, G_b [1/s] defines the perfusion rate, T_b [K] is the temperature of the blood, $Q_m(\boldsymbol{x})$ [W/m^3] denotes the metabolic heat source and $Q_J(\boldsymbol{x})$ [W/m^3] is the added heat source product of the radiofrequency induced thermal treatment.

In summary, a differential electric potential is applied to the electrodes which produces an electric potential in the tissue that is solved using Eq. (4). Once the potential is computed, the heating source due to the Joule heating effect is computed using Eq. (5). Finally, the temperature distribution is computed from Eq. (6) using the Joule heating source previously calculated. Fig. 1 shows the boundary conditions of the thermal model: a constant temperature along the cooling pad and an adiabatic condition on the remaining external boundaries.

2.1. FEM formulation

The radiofrequency thermal therapy problem characterized by Eqs. (4)–(6), are solved using the Finite Element Method (FEM). This method is expressed first in real variables and then followed by a complex variable representation.

The discrete form of Eq. (4) that describes the electric potential ϕ using the Galerkin method is given by

$$\mathbf{H}\boldsymbol{\phi} = \boldsymbol{q}. \tag{7}$$

where $\boldsymbol{\phi}$ is a vector of the electric potential at discrete points, $\boldsymbol{q}$ is a vector of loads (electric potential applied), and $\mathbf{H}$ is the system matrix defined by

$$H_{ij} = \int_\Omega \sigma \frac{\partial N_i}{\partial x_r}\frac{\partial N_j}{\partial x_r} dx. \tag{8}$$

where $N_i(\boldsymbol{x})$ is the standard Lagrange basis defined over the nodes of the element. The r index stands for the coordinate axes $(x_1, x_2) = (x, y)$, and summation is assumed over repeated indices. In a similar way the discrete form of the bioheat transfer equation is given by

$$(\mathbf{K} + \mathbf{M})\mathbf{T} = \mathbf{q_b} + \mathbf{q_m} + \mathbf{q_J}, \tag{9}$$

where $\mathbf{K}$ is the matrix due to diffusion, $\mathbf{M}$ and $\boldsymbol{q_b}$ the matrix and vector due to the blood the perfusion rate, $\mathbf{q_m}$ the metabolic heat source and $\mathbf{q_J}$ the Joule heating source These terms are defined as follows

$$K_{ij} = \int_\Omega \lambda(\boldsymbol{x})\frac{\partial N_i(\boldsymbol{x})}{\partial x_r}\frac{\partial N_j(\boldsymbol{x})}{\partial x_r} d\boldsymbol{x}, \tag{10}$$

$$M_{ij} = \int_\Omega B_b N_i(\boldsymbol{x}) N_j(\boldsymbol{x}) d\boldsymbol{x}, \tag{11}$$

$$\mathbf{q_{b_i}} = \int_\Omega B_b T_b N_i(\boldsymbol{x}) d\boldsymbol{x}, \tag{12}$$

$$\mathbf{q_{m_i}} = \int_\Omega Q_m(\boldsymbol{x}) N_i(\boldsymbol{x}) d\boldsymbol{x}, \tag{13}$$

$$\mathbf{q_{J_i}} = \int_\Omega Q_J(\boldsymbol{x}) N_i(\boldsymbol{x}) d\boldsymbol{x}, \tag{14}$$

where $B_b = \rho_b C_b G_b$. The energy that the tissue receives via the electric field is dissipated by the effect of the electrical resistivity of the material. Once the electric field is found from Eq. (7), the heat can be calculated by computing the gradient of the electric field, using Eq. (5), and then the temperature computed by solving the bioheat equation, Eq. (9).

3. Evaluation of sensitivities

A sensitivity analysis consists of determining the impact of a parameter on the output of a system. These parameters can be tissue properties, initial and boundary conditions. The selection of the method for computing sensitivities is not an easy task and key issues to be considered are the accuracy and the computational cost. It is also important that the differentiation scheme be easy to implement.

There are four main methods for computing the sensitivities. First, the direct differentiation method where the partial derivatives are derived analytically, the results from this method are exact. It is efficient only when the number of design variables is low (Choi and Kim [29]). Second, the adjoint method that can be thought of as the reverse of direct differentiation, where the derivative is calculated from the outputs rather than the inputs using the calculus of variations. This method is a feasible solution for problems with many design variables and few outputs where the direct differentiation becomes difficult to implement (Choi and Kim [29]). Third, automatic differentiation or computational differentiation that consist of the differentiation of the computer code itself. Automatic differentiation is based on the concept of the chain rule and the fact that a high-level function is composed of multiple smaller functions each having its own partial derivative and applying the chain rule of differentiation [30]. Fourth, the Finite Difference method (FDM) is a straightforward method for obtaining sensitivities as there is no need of code changes. The calculation of the sensitivities using the FDM consists of perturbing the variable of interest and recomputing the output, in order to determine the ratio of the change. The CTSE method is similar to the finite difference method as it uses a Taylor series expansion to approximate the derivative. However, CTSE method uses complex variable and the perturbation is made in the imaginary axis. It is easy to code, robust, accurate and does not suffer from subtraction error.

The Taylor series expansion of $f(x + ih)$ is defined as

$$f(x + ih) = f(x) + ihf'(x) - h^2\frac{f''(x)}{2} + O(h^3). \tag{15}$$

Taking the imaginary part of the $f(x + ih)$, that is, Im $(f(x + ih))$ neglecting the higher order terms and dividing by the step size (h) yields

$$f'(x) = \frac{\mathrm{Im}(f(x + ih))}{h} + O(h^2), \tag{16}$$

which is a second-order approximation of the first derivative. In other words, the information of the first derivative is found in the imaginary part of the function. As can be seen, Eq. (16) does not have a difference operation between two numbers. The step size should be extremely small in order to recover the exact numerical derivative. Additionally, the method is straightforward to implement in an existing FEM code. This can be accomplished by either using the native complex data type in a user-written code or by incorporating user-defined finite elements into a commercial code as it was done in [17]. Eq. (16) yields accurate numerical derivatives when h is very small, e.g., $h = 10^{-10}$.

Computing the derivative in this way requires that the variables are complex consisting of real and imaginary parts. This implies an increase in the memory and the computation time. Despite these apparent drawbacks, the accuracy, robustness and ease of implementation of the CTSE method make it a great option for calculating first order derivatives.

3.1. Implementation of the CTSE method into a finite element code

The conversion of a real-valued FEM solver into a complex valued FEM solver involves the transformation of each real number into complex. A complex number, $a + ib$, can be represented as a pair (a,b) and numerous languages support operations among complex numbers. Also, there are linear algebra modules with solvers that are capable of

handling complex variables. However, with the aim to support multi-complex analysis in the future, this implementation was made using the Cauchy-Riemann matrix representation for a complex number [31]. If z is a complex number and $z = a + ib$, then,

$$z := \begin{bmatrix} \mathrm{Re}(z) & -\mathrm{Im}(z) \\ \mathrm{Im}(z) & \mathrm{Re}(z) \end{bmatrix} = \begin{bmatrix} a & -b \\ b & a \end{bmatrix}. \tag{17}$$

In matrix form the real part is located along the diagonal of the matrix. Operations between complex numbers are transformed into standard matrix operations. The CTSE implementation was based on a standard finite element code using linear triangular elements. The real variables were turned into complex variables using the Cauchy-Riemann matrix notation. For example, a real valued element matrix $\mathbf{K}^e$ for a linear element is a 3×3 real matrix; for a complex matrix form it will be:

$$\mathbf{K}^e = \begin{bmatrix} \mathrm{Re}(K_{11}) & \mathrm{Re}(K_{12}) & \mathrm{Re}(K_{13}) & -\mathrm{Im}(K_{11}) & -\mathrm{Im}(K_{12}) & -\mathrm{Im}(K_{13}) \\ \mathrm{Re}(K_{21}) & \mathrm{Re}(K_{22}) & \mathrm{Re}(K_{23}) & -\mathrm{Im}(K_{21}) & -\mathrm{Im}(K_{22}) & -\mathrm{Im}(K_{23}) \\ \mathrm{Re}(K_{31}) & \mathrm{Re}(K_{32}) & \mathrm{Re}(K_{33}) & -\mathrm{Im}(K_{31}) & -\mathrm{Im}(K_{32}) & -\mathrm{Im}(K_{33}) \\ \mathrm{Im}(K_{11}) & \mathrm{Im}(K_{12}) & \mathrm{Im}(K_{13}) & \mathrm{Re}(K_{11}) & \mathrm{Re}(K_{12}) & \mathrm{Re}(K_{13}) \\ \mathrm{Im}(K_{21}) & \mathrm{Im}(K_{22}) & \mathrm{Im}(K_{23}) & \mathrm{Re}(K_{21}) & \mathrm{Re}(K_{22}) & \mathrm{Re}(K_{23}) \\ \mathrm{Im}(K_{31}) & \mathrm{Im}(K_{32}) & \mathrm{Im}(K_{33}) & \mathrm{Re}(K_{31}) & \mathrm{Re}(K_{32}) & \mathrm{Re}(K_{33}) \end{bmatrix} \tag{18}$$

Finally, the solutions of the different partial differential equations will result in a vector as

$$\mathbf{u} = \begin{bmatrix} \mathrm{Re}(u_1) \\ \mathrm{Re}(u_2) \\ \mathrm{Re}(u_3) \\ \mathrm{Im}(u_1) \\ \mathrm{Im}(u_2) \\ \mathrm{Im}(u_3) \end{bmatrix} = \begin{bmatrix} \mathrm{Re}(u_1) \\ \mathrm{Re}(u_2) \\ \mathrm{Re}(u_3) \\ \frac{\partial u_1}{\partial k} h \\ \frac{\partial u_2}{\partial k} h \\ \frac{\partial u_3}{\partial k} h \end{bmatrix}, \tag{19}$$

where the real part corresponds to the normal output of the system, whereas, the imaginary part divided by the step size h, will give us the sensitivity with respect to the variable that was perturbed by h in the imaginary direction. This result is general and can be applied to any type of finite element of two- or three-dimensional domains. In those cases, the number of degrees of freedom will change accordingly.

4. Numerical example

FEM and ZFEM implementations of the Joule heating and the bioheat transfer equation were developed in the Matlab ® language [32]. A simple geometric domain was selected to illustrate the capabilities of the method. This example, with the same geometry and boundary conditions, was used by Majchrzak et al. [27] and is presented in Fig. 1. Its dimensions are 0.08[m] in the x direction and 0.04[m] in the y direction. The electrodes are located at the upper and lower boundary from $x = 0.032$ to $x = 0.048$[m]. The tumor is represented as a square domain with size of 0.015[m] and its left inferior vertex has a coordinate of $x = 0.032$[m], $y = 0.016$[m]. The values of the properties used for the healthy and the tumor tissue are presented in the Table 1. The values of the properties for the human blood are listed in the Table 2.

For the purpose of this analysis, these properties were considered independent of the temperature. The boundary conditions for the electric potential were as follows

- $\phi_1 = 10$ [V] on Γ_1, the upper electrode.
- $\phi_1 = -10$ [V] on Γ_2, the lower electrode.
- $\partial\phi/\partial n = 0$ on $\Gamma_3 + \Gamma_4$, ideal insulation on the remaining external boundaries.

For the bioheat transfer the following boundary conditions were implemented

- $T_1 = 32.5$°C on Γ_1, Γ_2 and Γ_3; the cooling pad.
- $\partial T/\partial n = f = 0$ on Γ_4, zero heat flux on the remaining external boundaries.

The computation of sensitivities was accomplished using CTSE with a step size of $h = 10^{-10}$ for all parameters.

Table 1
Thermal and electrical properties of a healthy (Ω_1) and a carcinoma (Ω_2) human liver at a frequency of 100[kHz]. (Data source from references [33,34] and [35]).

Tissue	λ [W/m K]	G_b [1/s]	Q_m [W/m^3]	σ [s/m]
Ω_1	0.469	0.0005	4200	0.179
Ω_2	0.600	0.002	42000	0.461

Table 2
Thermal properties of the human blood. (Data source from reference [36]).

Temperature T_b [K]	Specific Heat C_b [J/kg K]	Density ρ_b [kg/m^3]
310.15	4180	1000

4.1. Methodology

Solving the radiofrequency induced thermal process involves three steps. (a) Given an electrical potential at the electrodes, solve for the electrical potential distribution in the whole domain, Eq. (4). (b) Determine the gradient of the electrical potential to compute the Joule heating source Eq. (5) (c) Given the Joule heating source, solve for the temperature distribution, Eq. (6). These two steady state equations were solved in a sequential fashion using the complex variable implementation of the FEM code.

The problem was solved using four different meshes in order to examine the convergence of the solution in the sensitivities. The coarsest mesh contained 496 elements, the next mesh contained 1984 elements, the third mesh contained 7936 elements, and the finest mesh consisted of 13,206 elements. The solution for the temperature at the center of the tumor and the relativity sensitivity of the temperature with respect to λ_1 at the center of the tumor was computed with each mesh and the results are compared in Fig. 2. It can be observed the asymptotic convergence of both solutions. The temperature result of the 1984 node mesh differs by 0.3% with respect to the finest mesh and the sensitivity result differs by 0.99%. The results for the 7936 node mesh differ by 0.04% for the temperature,

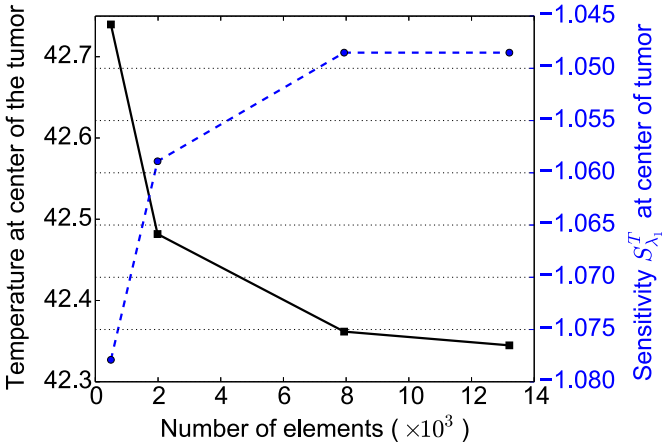

Fig. 2. Convergence analysis for the temperature and sensitivity with respect to λ evaluated at the center of the tumor tissue.

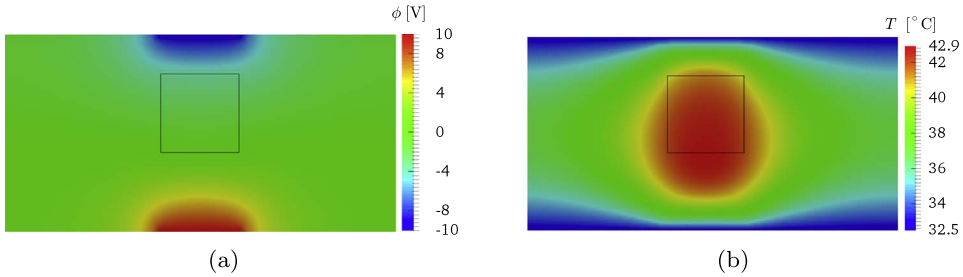

Fig. 3. Electric potential and temperature field of the radiofrequency induced thermal process. (a) Electric potential field ϕ[V], (b) Temperature field distribution T[°C].

and by 0% for the sensitivity, with respect to the results of the finest mesh.

Fig. 3 shows the electrical potential and the temperature distribution for the example problem. It is observed that using a voltage of −10 [V] and 10 [V] as boundary conditions, a maximum temperature of 42.9°C was obtained and was located in the tumor region of the domain. This temperature value is just below the recommended therapeutic value of 43°C.

At this point, in terms of the desired treatment, it is necessary to increase the temperature value at the tumor domain only. The procedure is to increase the difference in the electrical potential of the two electrodes. Furthermore, due to the delicate nature of the procedure, it is important to determine what is the effect of small variations of the different parameters involved in the heating of the tissue. Identifying the most critical factor and understanding the effect of the different variables in the radiofrequency induced thermal process will lead to better treatments using this technique.

4.2. Sensitivity analysis

The goal of the research is to determine the effect that the parameters and the tissues properties have on the temperature distribution. This information can be used to obtain the best treatment with a minimal collateral damage. Therefore, a sensitivity analysis for each parameter and property was carried out using CTSE. Since the sensitivity found by the CTSE method for each property is an absolute sensitivity which can not be compared, a relative sensitivity is used. It is defined as [37]

$$S_k^T(\boldsymbol{x}) = \frac{\partial T(\boldsymbol{x})/T(\boldsymbol{x})}{\partial k/k} = \frac{\partial \ln T(\boldsymbol{x})}{\partial \ln k} = \frac{k}{T(\boldsymbol{x})}\frac{\partial T(\boldsymbol{x})}{\partial k}, \tag{20}$$

where k represents an arbitrary parameter of the model. Eq. (20) provides a dimensionless value that can be used to compare the sensitivities obtained for all parameters. Fig. 4 presents the relative temperature sensitivities with respect to the thermal conductivity of the healthy (see Fig. 4a) and the tumor (see Fig. 4b) tissues; and with respect to the electrical conductivity of the healthy (see Fig. 4c) and the tumor (see Fig. 4d) tissues. It can be observed that these two properties have opposite effects on the temperature. Increasing the thermal conductivity will decrease the temperature and increasing the electric conductivity will increase the temperature. Also, the temperature is less sensitive to the thermal conductivity of the carcinoma than to the thermal conductivity of the healthy tissue, and its effect seems to be limited within the tumor region. The thermal conductivity of the healthy tissue acts as a diffuser, spreading the temperature across the domain. On the other hand, an increase in the electrical conductivity of the healthy tissue would lead to an increase in the temperature field on the tumor region as the Fig. 4c suggests. However, it will also increase the temperature in the healthy tissue and its maximum value will be in the healthy region.

The relative sensitivity is computed at each point in the domain $S_k^T(\boldsymbol{x}_j)$ with $\boldsymbol{x}_j \in \Omega$ representing a finite element node. In order to compare the sensitivities with respect to the different parameters its maximum value and average value over the total domain and over the tumor domain were calculated. That is, $\max(S_k^T(\boldsymbol{x}_j))$ and $\sum_j^N S_k^T(\boldsymbol{x}_j)/N$ for all $\boldsymbol{x}_j \in \Omega$, with N the total number of nodes in Ω, and $\max(S_k^T(\boldsymbol{x}_j))$ and $\sum_j^{N_2} S_k^T(\boldsymbol{x}_j)/N_2$ for all $\boldsymbol{x}_j \in \Omega_2$, and N_2 the total number of nodes in Ω_2. The results of the maximum and averaged relative sensitivities of the temperature with respect to different variables (electrical conductivity, perfusion rate, metabolic heat and the thermal conductivity for the healthy and carcinoma tissue) were calculated and the results are summarized in Table 3. The average sensitivity of the parameters on the tumor domain is plotted in Fig. 5. It can be observed that the electrical and the thermal conductivity of the healthy tissue are the two properties with the greatest impact on the temperature, with an average relative sensitivity value of $\sigma_1 = 1.246 \times 10^{-2}$ and $\lambda_1 = -1.242 \times 10^{-2}$ respectively. Furthermore, the thermal conductivity of the tumor, with $S_{\lambda_2}^T = -0.073 \times 10^{-2}$, and the electrical conductivity of the tumor, with $S_{\sigma_2}^T = 0.088 \times 10^{-2}$, seem not to have a significant influence on the temperature distribution even over the tumor region.

Boundary conditions model the effect of the surroundings on the object of interest. Their values are determined based on physical considerations or experimental measurements. Obviously, these data may have measurement error or uncertainty. Therefore, it is important to characterize how sensitive are the results to the boundary conditions. In order to compute these sensitivities, the following perturbations were applied to the boundary conditions:

- Electric field Dirichlet boundary condition: $\phi(\boldsymbol{x}) = 10 + i\ h$ at the top electrode, $\boldsymbol{x} \in \Gamma_1$.
- Temperature field Newman boundary condition: $\frac{\partial T(\boldsymbol{x})}{\partial n} = f = 0 + i\ h$ at the adiabatic boundary, $\boldsymbol{x} \in \Gamma_4$.
- Temperature field Dirichlet boundary condition: $T(\boldsymbol{x}) = 305.65 + i\ h$ at the cooling pad, $\boldsymbol{x} \in \Gamma_1 + \Gamma_3$.

The first analysis will provide the temperature sensitivity with respect to the applied voltage, $S_{\phi_{\Gamma_1}}^T$. The second one will provide the temperature sensitivity with respect to the heat flux through the boundary $S_{f_{\Gamma 4}}^T$. The third one will provide the temperature sensitivity with respect to the assumed, or measured, temperature at the cooling pad $S_{T_{\mathrm{CP}}}^T$ Table 4. The temperature sensitivities over the domain are shown in Fig. 6. Also, the maximum and average sensitivity over the total domain Ω and the tumor domain Ω_2 were calculated and are shown in Table 5. It can be observed that the temperature sensitivity with respect to the temperature boundary condition is 100% near to the cooling pad and decreases away from the boundary. This is an expected result as this boundary condition sets the temperature and therefore has a one-to-one effect on the temperature of the healthy tissue near to the cooling pad. Over the tumor region, the average sensitivity is 36.87% and the maximum is 53.56%. These are large values when compared to the sensitivities with respect to the other parameters. The value of this boundary condition comes from experimental measurement. Therefore, very accurate measurements have to be made in order to obtain accurate temperature values in the healthy and tumor tissues. The second most influential boundary condition is the electric potential boundary condition. This value can be controlled in the radiofrequency induced thermal procedure. An increase in the electric potential of the

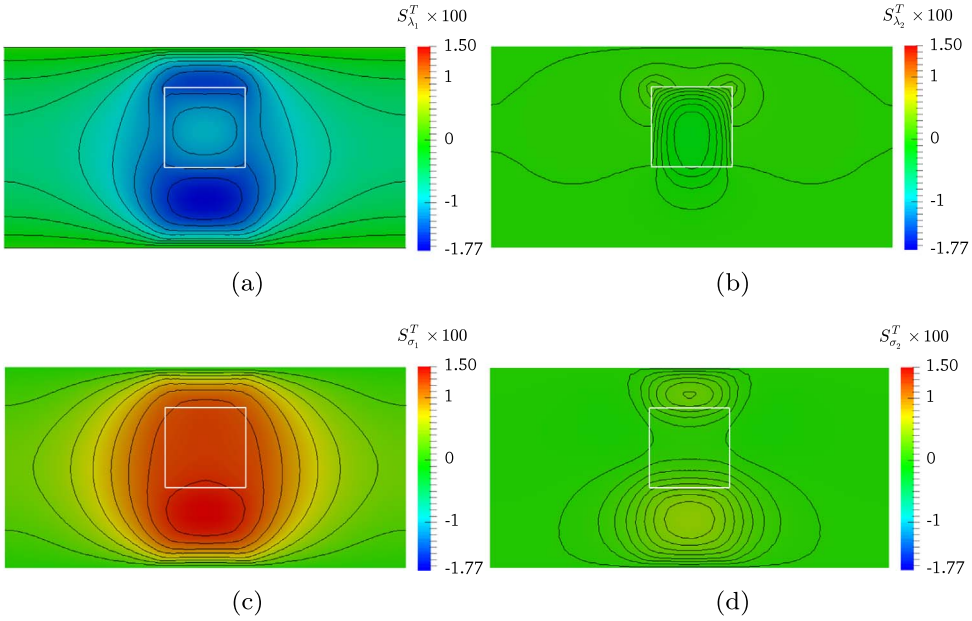

Fig. 4. Relative sensitivity of temperature with respect to: (a) thermal conductivity of the healthy tissue $S^T_{\lambda_1}$, (b) thermal conductivity of the tumor $S^T_{\lambda_2}$, (c) electrical conductivity of the healthy tissue $S^T_{\sigma_1}$, (b) electrical conductivity of the tumor $S^T_{\sigma_2}$.

Table 3
Average sensitivity of the temperature with respect to different properties. The values are multiplied by 100.

	Thermal conduct.		Perfusion rate		Metabolic heat		Electric conduct.	
Properties	λ_1	λ_2	G_{b1}	G_{b2}	Q_{m1}	Q_{m2}	σ_1	σ_2
Maximum sensitivity over Ω	−1.77	−0.203	−0.275	−0.807	0.320	0.785	1.500	0.432
Average sensitivity over Ω	−0.78	−0.002	−0.056	−0.180	0.170	0.18	0.624	0.050
Maximum sensitivity over Ω_2	−1.51	−0.203	−0.240	−0.807	0.200	0.785	1.370	0.260
Average sensitivity over Ω_2	−1.242	−0.073	−0.153	−0.646	0.138	0.642	1.246	0.088

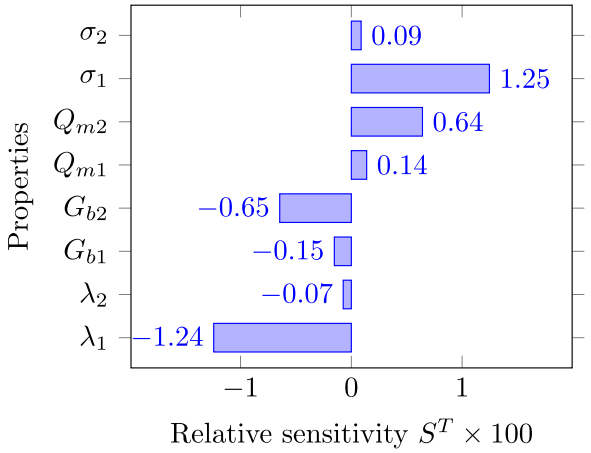

Fig. 5. Average tumor sensitivity of temperature with respect to the properties. The values are multiplied by 100.

electrodes will increase the temperature in the whole domain (0.67% on average) and its effect is larger inside the tumor (1.33% on average). Finally, the sensitivity with respect to the ideal adiabatic condition is high in the region near the boundary and where the temperature is low. However, at the tumor region, it has an average of 0.0755%. This value shows that the adiabatic condition is well imposed.

4.3. A comparison of CTSE against the FDM

In order to verify the accuracy of the complex Taylor series expansion method for the radiofrequency induced thermal procedure, the sensitivity of temperature with respect to two parameters (the thermal conductivity and the electrical conductivity of the healthy tissue) were calculated using the Finite Difference Method (FDM). The comparison was made for different step sizes (h), from $h = 1$ to $h = 1e^{-20}$.

Table 4
Average and maximum sensitivity of the temperature with respect to the boundary conditions. Values are multiplied by 100.

	Electric potential	Adiabatic boundary	Cooling Temp.
Maximum sensitivity over Ω	1.920	3.040	100.00
Average sensitivity over Ω	0.670	0.490	61.74
Maximum sensitivity over Ω_2	1.630	0.110	53.56
Average sensitivity over Ω_2	1.330	0.075	36.87

$$\varepsilon = \frac{\left| f' - f'_{ref} \right|}{\left| f'_{ref} \right|}, \tag{21}$$

where $f = \max_x(S^T_{\lambda 1}(x))$, The reference derivative was computed using the CTSE method with a step size of $h = 10^{-50}$. Fig. 7 and 8 plot the results of this comparison. It can be observed that in both cases, the sensitivity computed using the finite difference method fails at h values smaller than 10^{-12}. This is due to round-off errors involved in the calculation of the sensitivity caused by the subtraction of terms. On the

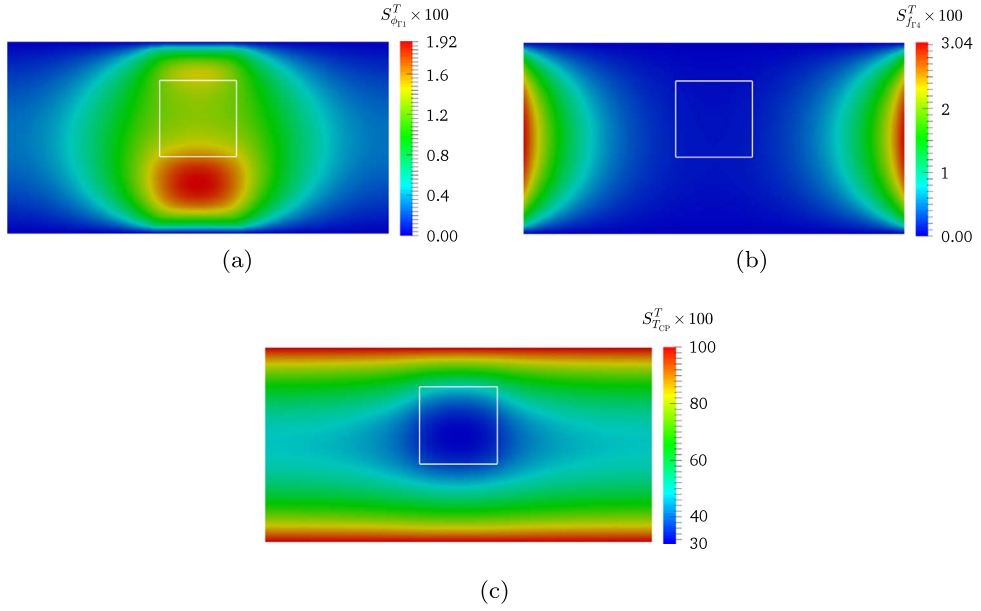

Fig. 6. Relative sensitivity of temperature with respect to the boundary conditions: (a) electrical Dirichlet boundary condition $S^T_{\phi_{\Gamma_1}}$, (b) ideal adiabatic boundary condition $S^T_{J_{\Gamma 4}}$, (c) temperature at the cooling pad $S^T_{T_{\mathrm{CP}}}$.

Table 5
Average and maximum sensitivity of the temperature with respect to the boundary conditions. Values are multiplied by 100.

	Electric potential	Adiabatic boundary	Cooling Temperature.
Maximum sensitivity over Ω	1.920	3.040	100.00
Average sensitivity over Ω	0.670	0.490	61.74
Maximum sensitivity over Ω_2	1.630	0.110	53.56
Average sensitivity over Ω_2	1.330	0.075	36.87

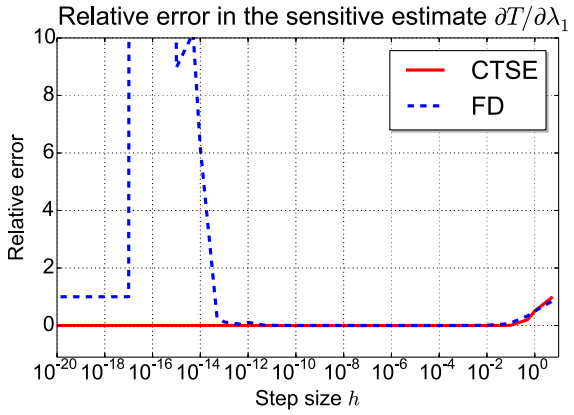

Fig. 7. Normalized error in the thermal conductivity sensitivity estimates $\partial T/\partial \lambda_1$, given by finite-difference and the complex Taylor series expansion method for different step sizes.

other hand, the sensitivity computed using the CTSE method remains constant throughout the entire range of the step size and oscillations are not present. As opposed to the finite difference method, the CTSE method still converges when very low step size values are used. Therefore, the sensitivity computed with the CTSE method is step size independent.

4.4. Computational efficiency

When using a complex-valued code the number of degrees of freedom are duplicated, causing an increase in the memory used and

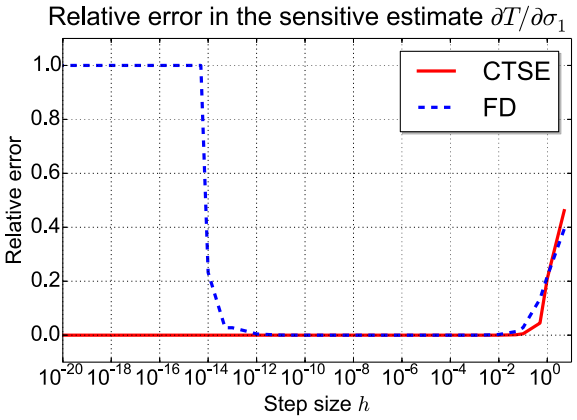

Fig. 8. Normalized error in the electrical conductivity sensitivity estimates $\partial T/\partial \sigma_1$, given by finite-difference and the complex Taylor series expansion method for different step sizes.

the solution time. The current implementation uses sparse matrices where only the elements different from zero are stored. The matrix size in a sparse matrix is the number of entries different from zero. Therefore, the memory requirements for the complex-value code will depend mainly on how the complex perturbation affects the matrix. For example, the sensitivity with respect to a boundary condition will only affect the system vector so the size of the sparse matrix is only increased by a factor of two (imaginary part equal zero in Eq. (18). On the other hand, if the sensitivity involves a perturbation in the full stiffness matrix then the size of the sparse matrix is increased by a factor of four. In order to assess the computational cost of a complex perturbation, these two extreme cases using eight different mesh densities were evaluated. Table 6 presents the results for the two types of sensitivities. a) Sensitivity with respect to a boundary condition (e.g. temperature boundary condition) and b) Sensitivities with respect to the material properties (e.g thermal conductivity). For each case, the CPU time and the memory used by the program were computed. It can be observed case a) that the memory required was doubled and the total computing time was increased by a factor of 1.61 on average when compared to a single FEM evaluation. In case b) the memory requirements were multiplied by a factor of 4. However, the solution

Table 6
Computing time and memory requirements for complex-coded FEM for: a) Boundary condition perturbation, b) Material property perturbation. Real-coded FEM requirements are presented for reference but they do not produce sensitivity information alone.

a) Dirichlet boundary condition complex perturbation

	Real			Complex			
Num. Elem.	DOF	Num. Pos. sparse	Total Time (s)	DOF	Num. Pos. sparse	Total Time (s)	Time ratio
24	20	106	0.44	40	212	0.72	1.62
96	63	379	1.75	126	758	2.83	1.62
384	221	1,429	6.95	442	2,858	11.28	1.62
1,536	825	5,545	27.74	1,650	11,090	44.85	1.62
6,144	3,185	21,841	110.72	6,370	43,682	178.27	1.61
24,576	12,513	86,689	441.17	25,026	173,378	713.76	1.62
98,304	49,601	345,409	1,778.88	99,202	690,818	2,846.58	1.60
1,572,864	788,225	5,510,401	28,420.28	1,576,450	11,020,802	45,611.86	1.60

b) System matrix complex perturbation

	Real			Complex			
Num. Elem.	DOF	Num. Pos. sparse	Total Time (s)	DOF	Num. Pos. sparse	Total Time (s)	Time ratio
24	20	106	0.46	40	424	0.75	1.62
96	63	379	1.82	126	1,516	2.94	1.62
384	221	1,429	7.21	442	5,716	11.68	1.62
1,536	825	5,545	28.76	1,650	22,180	46.52	1.62
6,144	3,185	21,841	114.32	6,370	87,364	185.05	1.62
24,576	12,513	86,689	457.20	25,026	346,756	741.62	1.62
98,304	49,601	345,409	1,778.88	99,202	1,381,636	2,978.00	1.67
1,572,864	788,225	5,510,401	28,420.28	1,576,450	22,041,604	48,147.97	1.69

time increased only by a factor of 1.64 on average. These results represent an improvement over the run-time increase reported in the literature for full matrix storage, e.g. Martins et al. [38] and Whitfield et al. [39] reported increases in run-time by a factor of 3. In addition, there are other potential approaches to improve the efficiency of the complex method as the so-called complex variable semi-analytical method [40].

4.4.1. Finite difference comparison

When forward or backward finite difference is used to compute a sensitivity one needs to solve the problem at two different points. The solution time is a factor of two and the truncation error is $O(h)$. When the central finite difference is used to improve the truncation error to $O(h^2)$, the problem needs to be solved at three different points. The increase in the solution time is a factor of three. In contrast, CTSE has a truncation error of $O(h^2)$ and the overhead time is only 1.6 times.

5. Liver ablation treatment sensitivities

Fig. 9 shows the geometry of a human liver that was used to illustrate the capabilities of the method. A sensitivity analysis of the radiofrequency ablation (RFA) process was undertaken in order to determine the influence of the parameters in the resulting tumor/tissue temperature. This example is based on the experimental and numerical study developed by Fuentes et al. [1]. The RFA procedure used consisted of a pulsed voltage emanating through a tri-cooled tip electrode. The electrode was run in impedance mode for 12 minutes per ablation and cooled with chilled water. The liver domain was subdivided into two domains the healthy tissue domain Ω_1 and the tumor domain Ω_2. The boundary was subdivided into the external boundary Γ_2 and the electrodes Γ_1 inside the tumor tissue. A 2D section of the liver was used for the analysis.

5.1. Liver properties

The liver properties were selected as follows. The electric conductivity of the healthy and tumor tissue at a frequency of 460 kHz were obtained from [35], the heat transfer conductivities from [1] and the Perfusion rates were from [41].

With regard of the metabolic heat transfer generation, the authors found no agreement in the literature. For example, a value of $Q_m = 1091$ W/m^3 for the healthy tissue is used by several authors like [42,43]. This value is based on the paper by Mitchell [44]. Elia [45] identified the specific resting metabolic rates of major organs and

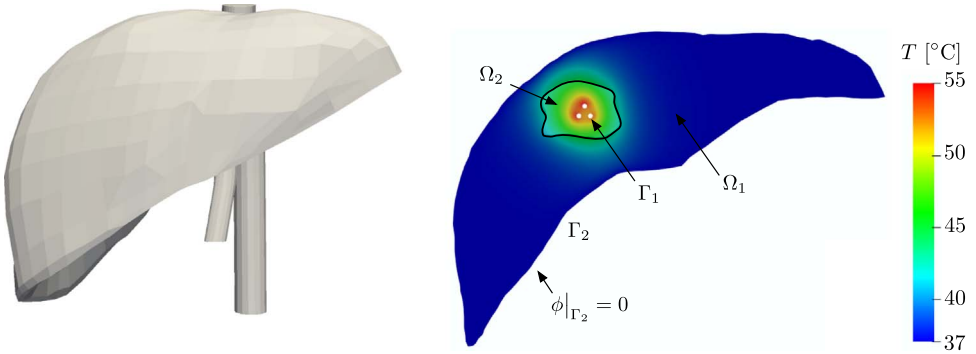

Fig. 9. 3D Liver geometry and a 2D section showing the resulting temperature of an radiofrequency ablation process. No cooling at the electrodes was considered in this case.

tissues in young adults with normal weight. A value of 9.7 W/m^3 was given for the liver. Fiala et al. [46] presented a computer model of human thermo-regulation for a wide range of environmental conditions. A metabolic rate of 4100 W/m^3 was given to the human viscera. Kummitha et al. [47] computed the Energy Expenditure (EE), for different organs/tissues, using information from mouse and a mathematical model. They proposed a metabolic heat rate for the liver of 10.8 W/m^3

No information was found relative to the liver tumor metabolic heat. However, Gautherie [48] used an electric analogy model of heat transfer in cancerous breast to determine the metabolic heat generation. He proposed a value of 450 W/m^3 for normal tissue and 29000 W/m^3 for cancer tissue. Also, Liu and Xu [49] recognized the lack of experimental measurements of this parameter and assumed a value of 420 W/m^3 for healthy and 4200 W/m^3 for tumor tissues underneath the skin. In [50], these values are multiplied by a factor of ten (no reason given). In spite of the uncertainty of these values, a number of articles use this source for the metabolic heat generation. [51,52] and [27] are examples of that.

Finally, some authors line Chang [6] assumed that the metabolic heat source was an insignificant influence in the ablation simulation and was not taken into account when solving the bioheat equation. Summarizing, the metabolic heat generation possible values are in a range from zero to 29000 W/m^3. Therefore, sensitivities of this parameter along the whole range need to be computed.

A summary of the properties of the healthy and tumor tissue are shown in Table 7 and the properties of the blood are shown in Table 2.

5.2. Boundary conditions

The electric potential as varied in a range in order to obtain the ablation temperatures. An electric potential of 15V, 20V, 30V was used at the electrodes Γ_1, and a zero potential at the external boundaries of the liver Γ_2.

The cooling at the electrodes was modelled as a thin cylinder with water inside. As the diameter is very small, 1 mm, the fluid can be consider laminar and the convective coefficient approximated as $h \approx 2000$ W/m^2. K [53]. The cooling temperature was set to 30 °C and the temperature at the external boundary Γ_2 was set to 37 °C.

5.3. Mesh convergence

The problem was solved using three different meshes in order to examine the convergence of the solution. The coarsest mesh contained 3009 elements, the second mesh contained 5505 elements, and the finest mesh consisted of 10,510 elements. Due to the unstructured nature of the mesh, the maximum norm of the temperature sensitivity with respect to λ was used to test the solution convergence. The results were 0.4145 using the mesh with 3009 elements; 0.4139 with 5505 elements; and 0.4137 with 10,510 elements. It is observed that the last two results differ only by 0.05%, which represents the relative error in the solution. Based on these results, the mesh with 5505 elements was selected for the present study.

5.4. Results

The first set of computational experiments was designed to test the sensitivity of the temperature to the metabolic heat generation. The voltage was 15 V and no cooling was considered. Table 8 shows the results obtained for the different ranges of metabolic heat. It can be observed that the maximum temperature changes only for very high values of Q_m and the change is about 1.3%. However, these high values have not been reported in liver cancer. It is also observed that local sensitivities obtained by CTSE are very small and therefore metabolic heat generation has a minor role in the ablation process.

Fig. 9 shows the temperature distribution for a voltage of 15 V and no cooling at the electrodes. In this case the maximum temperature at the tumor was 54.65 °C and the maximum temperature at the healthy tissue was 45.26 °C. It can be observed that the higher temperatures were concentrated in the tumor area. In contrast, Fig. 10 shows the temperature distribution for the same applied voltage but with cooling at the electrode tips. It can be observed that there is a region in the tumor in between the electrodes where the temperature does not reach values higher than 35 °C and therefore that part of the tumor will not be effectively treated. Also, the sensitivity map shows that the highest sensitive areas are precisely around the electrodes.

Based on the previous results, only the sensitivities with respect to the cooling temperature $S^T_{T_\infty}$, convective cooling coefficient S^T_h, electric potential boundary condition S^T_V, and electric conductivity of the healthy tissue $S^T_{\sigma_1}$ were calculated. Their maximum and averaged values were calculated over the complete domain and over the healthy and tumor domains. The results are summarized in Table 9. It can be observed that the parameter with the largest influence in the temperature is the cooling temperature as it directly prescribe the values of the temperature of the tissue in the vicinity of the electrodes. The second largest influence in the temperature is the electric potential applied. A variation of the potential will affect the temperature over the whole domain. Another important parameter is the electric conductivity of the healthy tissue σ_1. The relative sensitivity is about 5%. As this variable is not under control of the process, special care must be taken when designing an adequate radiofrequency induced thermal process as the main interest of the process is to raise the temperature of the tumor only. To accomplish this it will be desirable to increase the electrical conductivity value of the tumor. Some research in this direction includes the introduction of nanoparticles [51,2,1,54,55] which are capable of modifying the general properties into the tumor region and concentrating the energy.

Table 7
Physical properties of the liver healthy tissue and liver tumor tissue. Metabolic heat transfer is evaluated in a range. Data source is presented in Section 5.1.

Tissue	λ [W/m°K]	G_b [1/s]	Q_m [W/m^3]	σ [s/m]
Ω_1	0.5	0.018	0 to 4200	0.26
Ω_2	0.6	0.022	0 to 29000	0.504

Table 8
Sensitivity of the temperature with respect to the metabolic heat for different range of values. $Q_m(\Omega_1)$ is the metabolic heat for the healthy tissue and $Q_m(\Omega_2)$ for the tumor tissue.

	$Q_m(\Omega_1) - Q_m(\Omega_2)$ [W/m^3]			
	0 – 0	10–100	420–4200	450–29,000
maximum temp at tumor [°C]	54.65	54.65	54.70	55.04
maximum temp at healthy [°C]	45.26	45.26	45.30	45.50
maximum sensitivity at tumor [%]	0.00	0.00	0.02	0.13
maximum sensitivity at healthy [%]	0.00	0.00	0.01	0.08

6. Conclusions

Sensitivity analysis of the radiofrequency induced thermal process was accomplished using the complex Taylor series expansion finite element method. A finite element code was written to support complex variables using the Cauchy-Riemann matrix representation. Derivatives with respect to a parameter were obtained by perturbing the variable of interest by a small amount h along the imaginary axis and then computing the imaginary part of the result. This constitutes a major advantage when designing a medical treatment where the sensitivities with respect to all the variables have to be considered in order to design a robust and safe procedure.

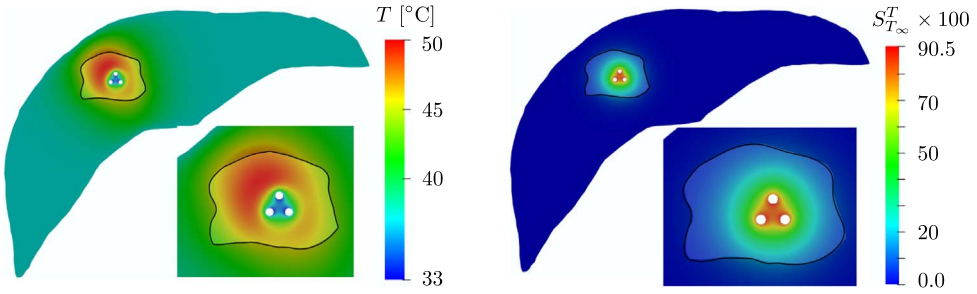

Fig. 10. Temperature distribution and temperature sensitivity for a 15 V RFA procedure and colling temperature of 30 °C at the electrodes.

Table 9
Maximum and average sensitivities computed over the liver Ω_1, tumor Ω_1, and healthy tissue Ω_2. The values are multiplied by 100.

	$S^T_{T_\infty}$	S^T_h	S^T_V	$S^T_{\sigma 1}$
Average sensitivity over Ω	16.29	−0.18	3.39	1.38
Average sensitivity over Ω_2	39.45	−0.45	7.36	3.21
Average sensitivity over Ω_1	1.21	−0.01	0.88	0.20
Maximum Sensitivity over Ω	90.48	0.00	10.75	4.85
Maximum sensitivity over Ω_2	90.48	−0.04	10.75	4.85
Maximum sensitivity over Ω_1	17.05	0.00	5.19	2.26

The electric field and bioheat equations were solved using the CTSE finite element code to automatically obtain sensitivity results. Relative sensitivities were computed and compared to establish the most influential properties in the radiofrequency induced thermal process. The parameters included the physical properties thermal, electrical conductivity, perfusion rate, metabolic heat, and heat capacity. The sensitives of the boundary conditions and cooling temperature were also computed.

It was found the thermal and electrical conductivity of the healthy tissue were the most influential properties in the final temperature. This means that if the thermal energy is not carefully applied to the right cancerous region healthy tissues can be damaged. It also supports the idea of locally and artificially changing these properties at the location of the tumor.

In the case of th RFA process, it was found that the highest relative sensitivity was the cooling temperature with values as high as 90%. The highest sensitivities were located in the area between the electrodes. As a consequence, when the low cooling temperatures are maintained, it will result in tumor areas not exposed to ablation temperature. The second largest temperature sensitivity was found to be with respect to the electric potential applied and a variation of the potential will affect the temperature over the whole domain. The metabolic heat transfers values for the liver and tumor are not well known. A sensitivity analysis in a different range of possible values revealed that there is no significant influence of the metabolic heat in the final ablation temperature.

The sensitivity of the temperature with respect to the thermal and electrical conductivity was compared with the finite difference method. The results showed that as opposed to the finite difference method, CTSE is step size independent. In contrast to the FDM, the CTSE only needs one run for each sensitivity of interest. The increase in run time for a complex FEA as compared to a real FEA was only 1.6; significantly lower than the 2x for forward/backward finite differencing or 3x for central differencing. Furthermore, the current CTSE implementation is efficient in memory and uses less computational time that finite difference method. CTSE has significant advantages in the sensitivity analysis computation. Once the finite element code is written with complex variables, it is easy to compute the sensitive of the variables of interest in a precise and robust manner. For this reason, the method is an excellent alternative to traditional sensitivity methods.

Appendix A. Supplementary data

Supplementary data associated with this article can be found in the online version at http://dx.doi.org/10.1016/j.finel.2017.07.001.

References

[1] D. Fuentes, R. Cardan, R.J. Stafford, J. Yung, G.D. Dodd, Y. Feng, High-fidelity computer models for prospective treatment planning of radiofrequency ablation with in vitro experimental correlation, J. Vasc. Interv. Radiol. 21 (11) (2010) 1725–1732. http://dx.doi.org/10.1016/j.jvir.2010.07.022.
[2] Y. Feng, D. Fuentes, Model-based planning and real-time predictive control for laser-induced thermal therapy, Int. J. Hyperth. 27 (8) (2011) 751–761.
[3] M.N. Rylander, Y. Feng, K. Zimmermann, K.R. Diller, Measurement and mathematical modeling of thermally induced injury and heat shock protein expression kinetics in normal and cancerous prostate cells, Int. J. Hyperth. 26 (8) (2010) 748–764.
[4] H.H. Pennes, Analysis of tissue and arterial blood temperatures in the resting human forearm, J. Appl. Physiol. 1 (2) (1948) 93–122.
[5] M. Tunç, U. Çamdali, S. Cikrikci, The bio-heat transfer equation and its applications in hyperthermia treatments, Eng. Comput. 23 (4) (2006) 451–463.
[6] I. Chang, U.D. Nguyen, Thermal modeling of lesion growth with radiofrequency ablation devices, Biomed. Eng. Online 3 (1) (2004) 27. http://dx.doi.org/10.1186/1475-925X-3-27.
[7] M. Zhang, Z. Zhou, S. Wu, L. Lin, H. Gao, Y. Feng, Simulation of temperature field for temperature-controlled radio frequency ablation using a hyperbolic bioheat equation and temperature-varied voltage calibration: a liver-mimicking phantom study, Phys. Med. Biol. 60 (24) (2015) 9455.
[8] Z. Wang, I. Aarya, M. Gueorguieva, D. Liu, H. Luo, L. Manfredi, L. Wang, D. McLean, S. Coleman, S. Brown, A. Cuschieri, Image-based 3d modeling and validation of radiofrequency interstitial tumor ablation using a tissue-mimicking breast phantom, Int. J. Comput. Assist. Radiol. Surg. 7 (6) (2012) 941–948. http://dx.doi.org/10.1007/s11548-012-0769-3 (URL ⟨http://dx.doi.org/10.1007/s11548-012-0769-3⟩).
[9] C. Schumann, C. Rieder, S. Haase, K. Teichert, P. S¨uss, P. Isfort, P. Bruners, T. Preusser, Interactive multi-criteria planning for radiofrequency ablation, Int. J. Comput. Assist. Radiol. Surg. 10 (6) (2015) 879–889. http://dx.doi.org/10.1007/s11548-015-1201-6 (URL ⟨http://dx.doi.org/10.1007/s11548-015-1201-6⟩).
[10] J.N. Lyness, C.B. Moler, Numerical differentiation of analytic functions, SIAM J. Numer. Anal. 4 (2) (1967) 202–210. http://dx.doi.org/10.1137/0704019.
[11] J.N. Lyness, Numerical algorithms based on the theory of complex variable, in: 1967 Proceedings of the 22nd National Conference, ACM '67, ACM, New York, NY, USA, 1967, pp. 125–133. http://dx.doi.org/10.1145/800196.805983.
[12] W. Squire, G. Trapp, Using complex variables to estimate derivatives of real functions, SIAM Rev. 40 (1) (1998) 110–112. http://dx.doi.org/10.1137/S003614459631241X.
[13] V. Vatsa, Computation of sensitivity derivatives of navier-stokes equations using complex variables, Adv. Eng. Softw. 31 (8–9) (2000) 655–659. http://dx.doi.org/10.1016/S0965-9978(00)00025-9.
[14] A. Voorhees, H. Millwater, R. Bagley, Complex variable methods for shape sensitivity of finite element models, Finite Elem. Anal. Des. 47 (10) (2011) 1146–1156.
[15] A. Voorhees, H. Millwater, R. Bagley, P. Golden, Fatigue sensitivity analysis using complex variable methods, Int. J. Fatigue 40 (2012) 61–73.
[16] D. Wagner, H. Millwater, 2D weight function development using a complex taylor series expansion method, Eng. Fract. Mech. 86 (2012) 23–37. http://dx.doi.org/10.1016/j.engfracmech.2012.02.006 (URL ⟨http://www.sciencedirect.com/science/article/pii/S0013794412000689⟩).
[17] H. Millwater, D. Wagner, A. Baines, K. Lovelady, Improved WCTSE method for the generation of 2D weight functions through implementation into a commercial finite element code, Eng. Fract. Mech. 109 (2013) 302–309. http://dx.doi.org/10.1016/j.engfracmech.2013.07.012 (URL ⟨http://www.sciencedirect.com/science/article/pii/S0013794413002579⟩).
[18] Z. Jing, X. Wu, Wide-range weight functions and stress intensity factors for arbitrarily shaped crack geometries using complex taylor series expansion method, Eng. Fract. Mech. 138 (2015) 215–232. http://dx.doi.org/10.1016/j.engfracmech.2015.03.006 (URL ⟨http://www.sciencedirect.com/science/article/pii/

S0013794415000788⟩).
[19] X.C. Zhao, X.R. Wu, D.H. Tong, Weight functions and stress intensity factors for pin-loaded single-edge notch bend specimen, Fatigue Fract. Eng. Mater. Struct. 38 (12) (2015) 1519–1528. http://dx.doi.org/10.1111/ffe.12343 (URL ⟨http://dx.doi.org/10.1111/ffe.12343⟩).
[20] A. Montoya, R. Fielder, A. Gomez-Farias, H. Millwater, Finite-element sensitivity for plasticity using complex variable methods, J. Eng. Mech. 141 (2) (2015) 04014118. http://dx.doi.org/10.1061/(ASCE)EM.1943-7889.0000837 (URL ⟨http://dx.doi.org/10.1061/(ASCE)EM.1943-7889.0000837⟩).
[21] A. Gomez-Farias, A. Montoya, H. Millwater, Complex finite element sensitivity method for creep analysis, Int. J. Press. Vessel. Pip. 132–133 (2015) 27–42. http://dx.doi.org/10.1016/j.ijpvp.2015.05.006 (URL ⟨http://www.sciencedirect.com/science/article/pii/S0308016115000587⟩).
[22] W.K. Anderson, J. Newman, D.L. Whitfield, Sensitivity analysis for navier-stokes equations on unstructured meshes using complex variables, AIAA J. 39 (1) (2001) 56–63.
[23] J.C. Newman, E.J. Whitfield, W.K. Anderson, Step-size independent approach for multidisciplinary sensitivity analysis, J. Aircr. 40 (3) (2003) 566–573 (URL ⟨http://arc.aiaa.org/doi/pdf/10.2514/2.3131⟩).
[24] B. Wang, A. Apte, Complex variable method for eigensolution sensitivity analysis, AIAA J. 44 (12) (2006) 2958–2961.
[25] J. Garza, H. Millwater, Multicomplex newmark-beta time integration method for sensitivity analysis in structural dynamics, AIAA J. 53 (5) (2015) 1188–1198. http://dx.doi.org/10.2514/1.J053282 (URL ⟨http://dx.doi.org/10.2514/1.J053282⟩).
[26] S. Kim, J. Ryu, M. Cho, Numerically generated tangent stiffness matrices using the complex variable derivative method for nonlinear structural analysis, Comput. Methods Appl. Mech. Eng. 200 (1–4) (2011) 403–413. http://dx.doi.org/10.1016/j.cma.2010.09.004 (URL ⟨http://www.sciencedirect.com/science/article/pii/S0045782510002549⟩).
[27] E. Majchrzak, G. Dziatkiewicz, M. Paruch, The modelling of heating a tissue subjected to external electromagnetic field, Acta Bioeng. Biomech. 10 (2) (2008) 29–37.
[28] D.J. Griffiths, Introduction to Electrodynamics, 4th ed., Pearson, Boston, 2013.
[29] K.K. Choi, N.-H. Kim, Structural Sensitivity Analysis and Optimization 1: Linear Systems, Springer, 2005. http://dx.doi.org/10.1007/b138709.
[30] L.B. Rall, Automatic Differentiation: Techniques and Applications, Springer, Berlin, 1981.
[31] G.B. Price, An Introduction to Multicomplex Spaces and Functions, CRC Press, New York, 1990.
[32] The MathWorks Inc., MATLAB and Statistics Toolbox Release 2015a, Natick, Massachusetts, United States, 2015.
[33] T.E. Cooper, G.J. Trezek, A probe technique for determining the thermal conductivity of tissue, J. Heat. Transf. 94 (2) (1972) 133–140.
[34] J. Valvano, J. Cochran, K. Diller, Thermal conductivity and diffusivity of biomaterials measured with self-heated thermistors, Int. J. Thermophys. 6 (3) (1985) 301–311. http://dx.doi.org/10.1007/BF00522151.
[35] D. Haemmerich, D.J. Schutt, A.W. Wright, J.G. Webster, D.M. Mahvi, Electrical conductivity measurement of excised human metastatic liver tumours before and after thermal ablation, Physiol. Meas. 30 (5) (2009) 459–466. http://dx.doi.org/10.1088/0967-3334/30/5/003.
[36] S. Tungjitkusolmun, Three-dimensional finite-element analyses for radio-frequency hepatic tumor ablation, IEEE Trans. Bio-Med. Eng. 49 (1) (2002) 3–9.
[37] T.F. Edgar, D.M. Himmelblau, Optimization of Chemical Processes, 2nd ed., McGraw-Hill, New York, 2001.
[38] J.R.R.A. Martins, P. Sturdza, J.J. Alonso, The complex-step derivative approximation, ACM Trans. Math. Softw. 29 (3) (2003) 245–262.
[39] D. Whitfield, J. Newman, W. Anderson, Step-size independent approach for multidisciplinary sensitivity analysis, Journal of aircraft 40 (3).
[40] W. Jin, B.H. Dennis, B.P. Wang, Improved sensitivity analysis using a complex variable semi-analytical method, Struct. Multidiscip. Optim. 41 (3) (2010) 433–439.
[41] B.E. Van Beers, I. Leconte, R. Materne, A.M. Smith, J. Jamart, Y. Horsmans, Hepatic perfusion parameters in chronic liver disease: dynamic ct measurements correlated with disease severity, Am. J. Roentgenol. 176 (3) (2001) 667–673.
[42] K.N. Rai, S.K. Rai, Effect of metabolic heat generation and blood perfusion on the heat transfer in the tissues with a blood vessel, Heat. Mass Transf. 35 (1) (1999) 75–79. http://dx.doi.org/10.1007/s002310050300 (URL ⟨http://dx.doi.org/10.1007/s002310050300⟩).
[43] P.K. Gupta, J. Singh, K. Rai, Numerical simulation for heat transfer in tissues during thermal therapy, J. Therm. Biol. 35 (6) (2010) 295–301. http://dx.doi.org/10.1016/j.jtherbio.2010.06.007 (URL ⟨http://www.sciencedirect.com/science/article/pii/S030645651000063X⟩).
[44] J.W. Mitchell, T.L. Galvez, J. Hengle, G.E. Myers, K.L. Siebecker, Thermal response of human legs during cooling, J. Appl. Physiol. 29 (6) (1970) 859–865.
[45] M. Elia, Organ and tissue contribution to metabolic rate, Energy metabolism: tissue determinants and cellular corollaries, 1992 (1992) 19–60.
[46] D. Fiala, K.J. Lomas, M. Stohrer, A computer model of human thermoregulation for a wide range of environmental conditions: the passive system, J. Appl. Physiol. 87 (5) (1999) 1957–1972 (URL ⟨http://jap.physiology.org/content/87/5/1957⟩).
[47] C.M. Kummitha, S.C. Kalhan, G.M. Saidel, N. Lai, Relating tissue/organ energy expenditure to metabolic fluxes in mouse and human: experimental data integrated with mathematical modeling, Physiol. Rep. 2 (9) (2014) e12159. http://dx.doi.org/10.14814/phy2.12159 (URL ⟨http://www.ncbi.nlm.nih.gov/pmc/articles/PMC4270223/⟩).
[48] M. Gautherie, Thermopathology of breast cancer: measurement and analysis of in vivo temperature and blood flow, Ann. N. Y. Acad. Sci. 335 (1) (1980) 383–415.
[49] J. Liu, L.X. Xu, Boundary information based diagnostics on the thermal states of biological bodies, Int. J. Heat. Mass Transf. 43 (16) (2000) 2827–2839.
[50] Z.-S. Deng, J. Liu, Monte carlo method to solve multidimensional bioheat transfer problem, Numer. Heat. Transf.: Part B: Fundam. 42 (6) (2002) 543–567.
[51] Y.-G. Lv, Z.-S. Deng, J. Liu, 3-d numerical study on the induced heating effects of embedded micro/nanoparticles on human body subject to external medical electromagnetic field, IEEE Trans. Nanobiosci. 4 (4) (2005) 284–294.
[52] Z.-S. Deng, J. Liu, Mathematical modeling of temperature mapping over skin surface and its implementation in thermal disease diagnostics, Comput. Biol. Med. 34 (6) (2004) 495–521.
[53] T.L. Bergman, F.P. Incropera, Introduction to Heat Transfer, John Wiley & Sons, New Jersey, 2011.
[54] Y. Feng, D. Fuentes, A. Hawkins, J. Bass, M.N. Rylander, A. Elliott, A. Shetty, R.J. Stafford, J.T. Oden, Nanoshell-mediated laser surgery simulation for prostate cancer treatment, Eng. Comput. 25 (1) (2009) 3–13.
[55] Y. Feng, M. Rylander, J. Bass, J. Oden, K. Diller, Optimal design of laser surgery for cancer treatment through nanoparticle-mediated hyperthermia therapy, in: NSTI-Nanotech, vol. 1, 2005, pp. 39–42.